iScience

CellPress
OPEN ACCESS

Article

GRP94 promotes anoikis resistance and peritoneal metastasis through YAP/TEAD1 pathway in gastric cancer

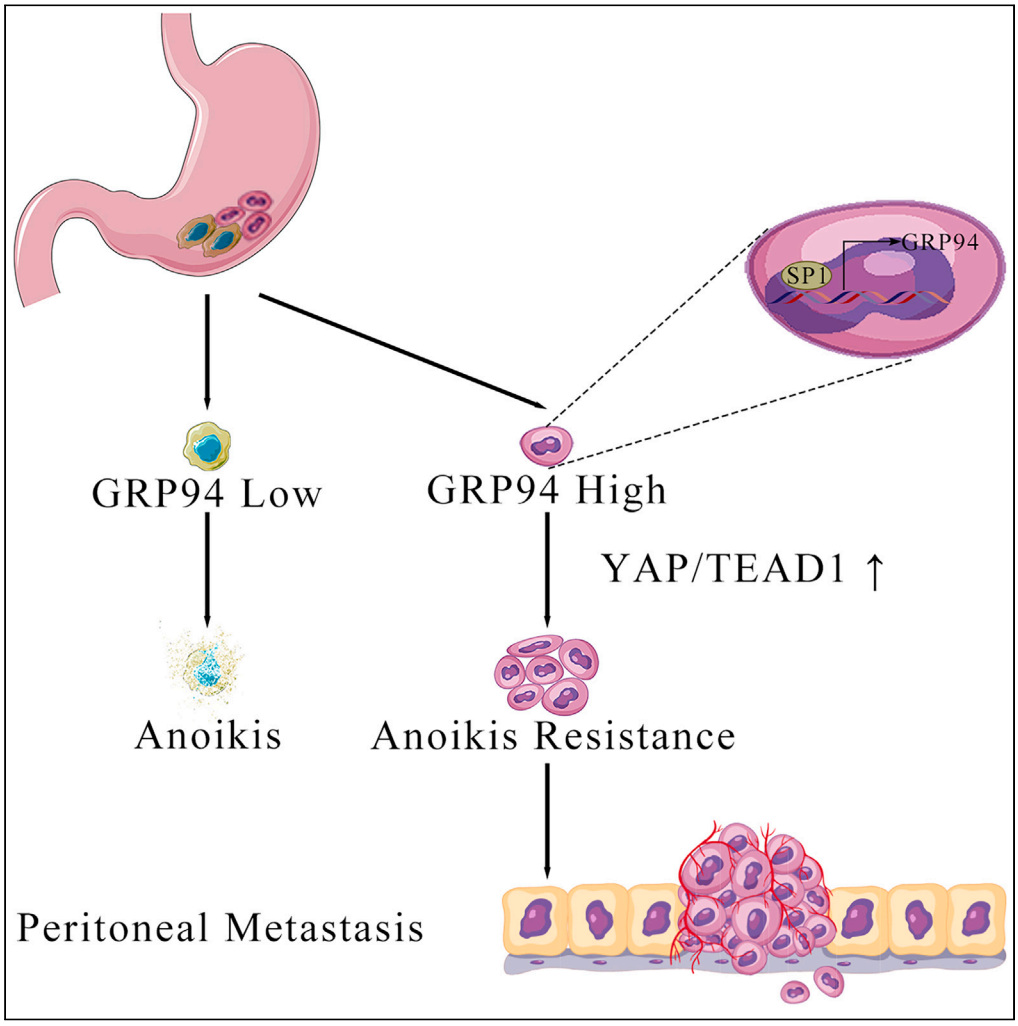

Qimeng Shi, Yang Lu, Yutong Du, ..., Yingyan Yu, Zhenqiang Wang, Chen Li

wzq12326@rjh.com.cn (Z.W.)
leedoctor@sina.com (C.L.)

Highlights

GRP94 enhances anoikis resistance, migration, and invasion in GC

GRP94 promotes metastasis by activating IL-6/YAP/TEAD1 pathway

Transcription factor SP1 leads to the upregulation of GRP94

Shi et al., iScience 27, 110638
September 20, 2024
https://doi.org/10.1016/j.isci.2024.110638

iScience

CellPress
OPEN ACCESS

Article

GRP94 promotes anoikis resistance and peritoneal metastasis through YAP/TEAD1 pathway in gastric cancer

Qimeng Shi,[1,2] Yang Lu,[1,2] Yutong Du,[1] Ruixin Yang,[1] Yingxin Guan,[1] Ranlin Yan,[1] Yingyan Yu,[1] Zhenqiang Wang,[1,*] and Chen Li[1,3,*]

SUMMARY

Anoikis resistance allows cancer cells to avoid death caused by detachment from the extracellular matrix's adhesion, enabling these cells to infiltrate and migrate to regions such as the peritoneum. This study emphasizes GRP94's involvement in anoikis resistance and peritoneal metastasis in gastric cancer (GC). It's found that GRP94 overexpression, linked to poor prognosis, was potentially due to SP1 and *GRP94* promoter interactions, confirmed through dual luciferase reporter (DLR), chromatin immunoprecipitation (ChIP), and quantitative real-time PCR (real-time qPCR). Increased GRP94 enhanced GC cells' anoikis resistance and metastasis. Decreasing GRP94 had opposite effects, potentially through yes-associated protein (YAP)/TEAD1 axis inhibition, with raised YAP phosphorylation and decreased TEAD1 levels detected by western blotting (WB). Inhibiting YAP counteracted GRP94's effects on anoikis resistance and metastasis, while activating YAP reversed the effects of GRP94 reduction. Animal experiments verified GRP94's contribution to GC's peritoneal metastasis. In conclusion, our work highlights the effect of GRP94 on anoikis resistance, showing potential value in treating peritoneal metastasis of GC.

INTRODUCTION

China experiences a significant prevalence of gastric cancer (GC), with an estimated 400,000 new cases annually. Remarkably, 30% of these cases are metastatic GC, a statistic that's been rising annually, underscoring both a high incidence and mortality rate.[1,2] Metastasis and recurrence are important causes of death in advanced GC patients, with peritoneal metastasis being the primary factor affecting the prognosis and recurrence of GC patients. The prognosis of patients with GC peritoneal metastasis is extremely poor, with a 5-year survival rate of less than 5%.[3]

Anoikis resistance plays a pivotal role in peritoneal metastasis within malignant tumors. This resistance allows tumor cells to bypass the extracellular matrix's adhesion dependency, warding off cell death triggered by detachment, and enabling these cells to infiltrate and migrate to regions such as the peritoneum.[4] However, the intricate regulatory systems that allow GC to sustain this trait remain somewhat enigmatic.

Yes-associated protein (YAP), integral to the Hippo-YAP signaling pathway, is implicated in the promotion of GC's peritoneal metastasis.[5,6] Given that YAP can be activated by cell adhesion molecules, it invites exploration into its relationship with anoikis resistance.[7,8] This area, however, presents conflicting views. For instance, Shao et al.[9] highlighted that inhibiting YAP, targeted by miR-200a, led cells to circumvent anoikis by reducing proapoptotic protein (p73, Noxa, Bax, and Bim included) levels in breast cancer. In contrast, A.K. Sood's team[10] identified YAP, when dephosphorylated by RhoA-activated MYPT1-PP1 phosphatase, as an enhancer of anoikis resistance in ovarian and colorectal cancer. The exact mechanism behind YAP's influence on anoikis resistance in GC remains ambiguous, necessitating further inquiry.

Glucose-regulated protein 94 (GRP94, alternatively labeled as HSP90B1) is typically stress-induced and is part of the heat-shock protein 90 (Hsp90) family. Predominantly found in the endoplasmic reticulum, it is acknowledged as a modulator of its client proteins' stability and function. Notably, GRP94 is closely tied to cellular resistance to stress, apoptosis, proliferation, invasion, inflammation, and immunity.[11,12] Surprisingly, deviating from initial assumptions, GRP94 levels were observed to decrease in circulating tumor cells of prostate cancer, suggesting that GRP94 might counteract tumor cells' resistance to anoikis.[13] The potential link between GRP94 and YAP remains largely unexplored, emphasizing the need for a deeper investigation into the interplay among GRP94, YAP, and anoikis resistance in GC.

Our study explores GRP94's role in GC, showing its impact on anoikis resistance and metastasis through the YAP/TEAD1 pathway. This perspective diverges from conventional views, offering insights into how cancer cells elude their inherent fate post-detachment and migrate

[1]Department of General Surgery, Shanghai Key Laboratory of Gastric Neoplasms, Shanghai Institute of Digestive Surgery, Ruijin Hospital, Shanghai Jiao Tong University School of Medicine, Shanghai 200025, People's Republic of China
[2]These authors contributed equally
[3]Lead contact
*Correspondence: wzq12326@rjh.com.cn (Z.W.), leedoctor@sina.com (C.L.)
https://doi.org/10.1016/j.isci.2024.110638

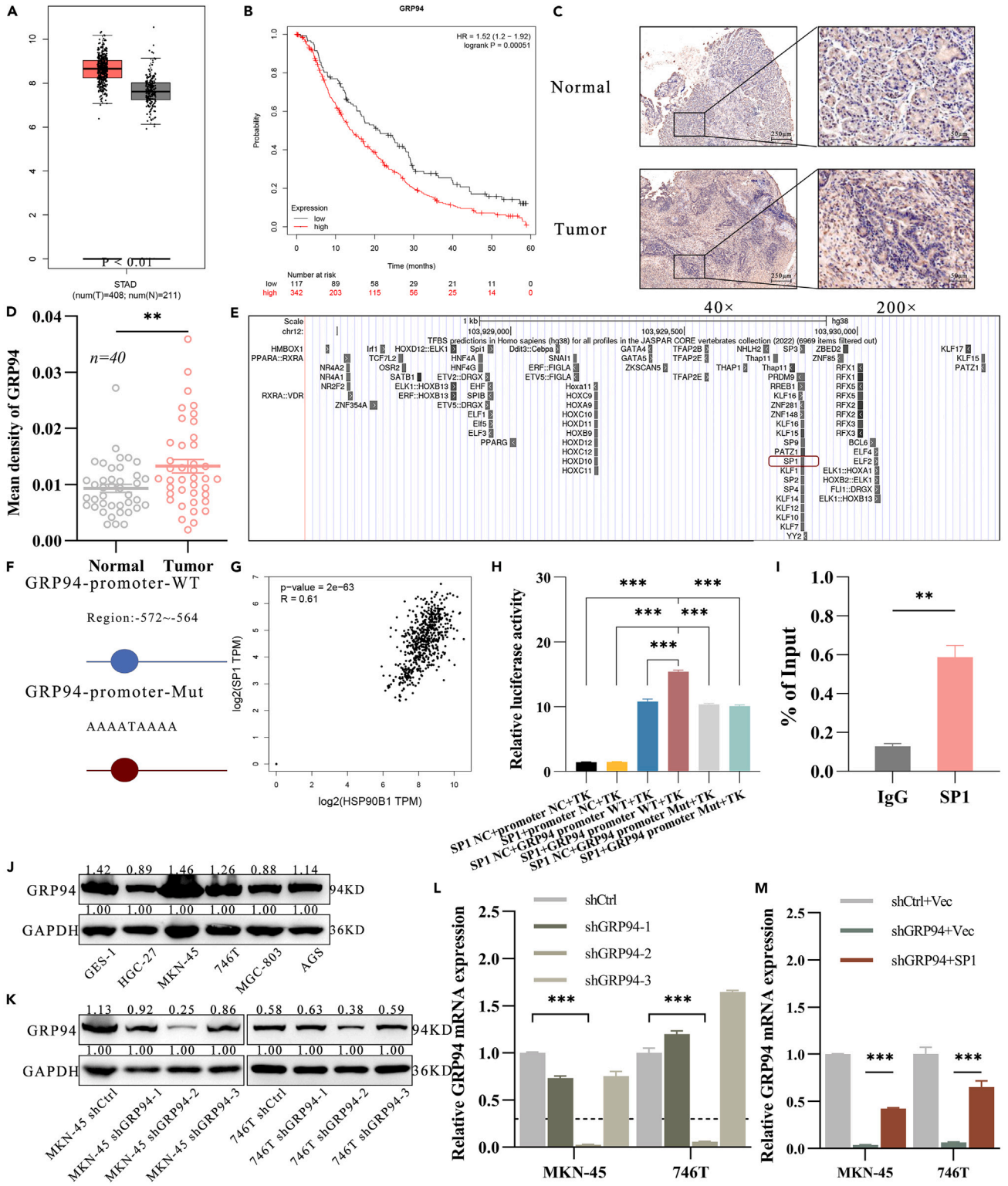

Figure 1. Expression of GRP94 was upregulated in tumor tissues in GC

(A) *GRP94* expression was assessed using GEPIA2 in stomach adenocarcinoma (STAD) samples (red, T = 408) compared to normal tissue samples (gray, *N* = 211) from both TCGA and GTEx projects.

Figure 1. *Continued*

(B) Kaplan-Meier plotter validation of *GRP94* expression in STAD patients yielded a log rank *p* value of 0.00051. GSE62254 was excluded according to Kaplan-Meier plotter's suggestion because it had markedly different characteristics than the other datasets. Outlier arrays were also excluded during quality control.

(C) IHC staining highlighted GRP94 protein levels differences between tumor tissues and their matched adjacent non-tumor tissues in GC. The left image has a scale bar of 250 μm at 40× magnification, while the right image has a scale bar of 50 μm at 200× magnification.

(D) The graph represents the quantification of the mean density of GRP94 levels in both groups ($n = 40$).

(E) UCSC data identified potential transcription factor binding sites in the promoter region of *GRP94*.

(F) JASPAR predicted the best SP1 binding site within *GRP94*'s promoter region.

(G) The chart displayed correlations among the expressions of *SP1* and *GRP94*.

(H) A dual luciferase reporter assay was performed on HGC-27 cells, and luciferase activity was assessed 48 h post-transfection.

(I) ChIP-qPCR confirmed the direct interactions between SP1 and *GRP94*.

(J) Western blot (WB) analysis confirmed the levels of GRP94 protein in the normal gastric epithelial cell line (GES-1) and various GC cell lines, including HGC-27, MKN-45, 746T, MGC-803, and AGS.

(K and L) WB and real-time qPCR were conducted to assess the efficiency of GRP94 knockdown in MKN-45 and 746T cells.

(M) Overexpression plasmids were used to evaluate the effect of upregulating SP1 on GRP94 expression in MKN-45 and 746T cells. (ns, $*p < 0.05$; $**p < 0.01$; $***p < 0.001$. All results are presented as mean ± SEM.).

elsewhere. A profound understanding of GC's peritoneal metastasis mechanism, coupled with innovative preventive and treatment strategies, is imperative for enhancing the prognosis of metastatic GC patients.

RESULTS

Expression of GRP94 was upregulated in tumor tissues in GC

Initially, based on the Gene Expression Profiling Interactive Analysis (GEPIA) database,[14] we observed that *GRP94* is expressed at higher levels in tumor tissues compared to normal tissues (Figure 1A). To determine whether this overexpression positively impacts patient prognosis, we conducted a survival analysis using Kaplan-Meier plotter (www.kmplot.com). The results revealed that the survival probability for the high-expression *GRP94* group was significantly lower compared to the low-expression *GRP94* group (log rank $p = 0.00051$) (Figure 1B). This discrepancy corresponded to a hazard ratio (HR) of 1.52 (1.2–1.92). An immunohistochemistry (IHC) analysis was carried out to compare GRP94 levels in tumor tissues and adjacent non-tumor tissues from 40 GC patients, further confirming the findings from the GEPIA database (Figures 1C and 1D). GRP94 levels in primary tumors and adjacent peritoneal metastasis were detected using the same method in six patients, and GRP94 in peritoneal metastasis showed a higher level (Figure S1). Interestingly, we discovered binding sites for SP1, rather than heat shock transcription factors (a family of transcription factors regulating the response of heat shock proteins to various proteotoxic stressors), in the core promoter region upstream of *GRP94* (Figure 1E). SP1, a critical member of the SP/KLF family, binds to the GC box, a prominent *cis*-regulatory element, with high specificity. This transcription factor is involved in various cancer cell functions, including apoptosis,[15] proliferation,[16] migration,[17] and invasion.[18] According to predictions from the JASPAR CORE database, the binding sites for SP1 are located at −572 to -564 (Figure 1F). Data from the GEPIA database indicate a strong correlation between *SP1* expression and *GRP94* in GC tissues ($r = 0.61$, $p < 0.001$) (Figure 1G). To investigate the direct interaction between SP1 and the *GRP94* promoter, we generated luciferase reporters with mutated *GRP94* promoter binding sites. Reduced luciferase activity in mutant *GRP94* promoter vectors suggests SP1's role in activating *GRP94* transcription (Figure 1H). This proposed interaction was further substantiated *in vivo* through chromatin immunoprecipitation combined with real-time qPCR (ChIP-qPCR) (Figure 1I). Among various clinicopathologic indicators, Borrmann type showed a significant association with GRP94 expression ($p = 0.0247$) (Table 1). GRP94 was silenced in MKN-45 and 746T cells. Subsequent experiments utilized MKN-45-shGRP94-2 and 746T-shGRP94-2, as selected based on real-time qPCR and WB outcomes (Figures 1J–1L). MKN-45-shGRP94 and 746T-shGRP94 cells were transfected with SP1 overexpression plasmids, resulting in upregulation of GRP94, as shown by real-time qPCR (Figure 1M).

Knockdown of GRP94 suppressed anoikis resistance, migration, and invasion of GC cells *in vitro*

Anoikis resistance, considered a fundamental requirement, allows tumor cells to survive in dynamic tumor microenvironments and migrate after detaching from their primary location.[19,20] Cells that adhere and subsequently proliferate in a standard 6-well plate after 7 days of suspension culture are characterized as anoikis-resistant. WB revealed that, post 7-day suspension culture, the GRP94 protein level in MKN-45 cells exceeded that observed after a 2-day suspension, indicating a potential role of GRP94 in GC cells' resistance to anoikis (Figure S2A). We then transfected MKN-45 and 746T cells with shGRP94 and its control vector, shCtrl. A notable difference in apoptosis rates between shCtrl and shGRP94 groups was detected, using flow cytometry, during suspension culture (MKN-45: 12.77% vs. 16.97%, $p < 0.001$; 746T: 41.17% vs. 61.03%, $p < 0.001$) but not in adherent cultures (Figures 2A and 2B). Ethd-1/calcein blue AM staining showed an obvious increase in apoptosis rate, due to the knockdown of GRP94, during suspension culture (MKN-45: 10.70% vs. 31.42%, $p < 0.001$; 746T: 55.71% vs. 71.97%, $p < 0.001$) (Figures 2C and 2D). Further tests involving wound healing, and Transwell migration and invasion assays were conducted to gauge GRP94's influence on the migratory and invasive capacities of these cancer cells. The wound healing assay revealed slower closure rates for wounds in MKN-45-shGRP94 and 746T-shGRP94 compared to their control counterparts (Figures 2E and 2F). The Transwell assay also showed a diminished cell passage through the membrane, irrespective of the presence of matrigel, in the shGRP94 groups compared to shCtrl groups (Figures 2G and 2H).

Table 1. Correlations between the expression of GRP94 and clinicopathologic parameters in GC patients

Clinicopathologic parameters	Case (*n* = 40)	GRP94 High (*n* = 26)	GRP94 Low (*n* = 14)	*p* value
Gender				
Male	28	18	10	>0.9999
Female	12	8	4	
Age				
≥60	28	20	8	0.1929
<60	12	6	6	
Tumor size				
≥5 cm	22	15	7	0.6409
<5 cm	18	11	7	
Differentiation				
Well, moderately	11	6	5	0.3932
Poorly, undifferentiated	29	20	9	
Borrmann type				
I	4	1	3	0.024
II	4	3	1	
III	27	21	6	
IV	5	1	4	
Lauren's classification				
Intestinal	22	16	6	0.6211
Diffuse	6	4	2	
Mixed	8	4	4	
Unclassifiable	4	2	2	
Local invasion				
T1+T2	5	4	1	0.6404
T3+T4	35	22	13	
Lymph node metastasis				
N0+N1	10	8	2	0.4457
N2+N3	30	18	12	
Pathological stage				
I + II	9	7	2	0.4527
III+IV	31	19	12	

Samples exhibiting greater GRP94 expression in tumor tissues, relative to adjacent non-tumor control tissues, were categorized into the high-expression group (*n* = 26). Conversely, those with lesser or equivalent expression were designated to the low-expression group (*n* = 14). A Chi-square or Fisher's exact test was utilized to determine the correlation between GRP94 expression and clinicopathological characteristics in GC patients.

Overexpression of GRP94 enhanced anoikis resistance, migration, and invasion in GC cells *in vitro*

Elevated levels of GRP94 led to a higher survival rate of detached HGC-27-GRP94 cells during suspension culture compared to HGC-27-Vec, with the apoptosis rate reducing from 23.90% to 15.73% ($p < 0.01$) (Figures 3A and 3B). The Ethd-1/calcein blue staining experiment was similar, and the results showed that overexpression of GRP94 led to a decrease in the apoptosis rate of HGC-27 cells from 29.16% to 17.06% (Figures 3C and 3D). The wound healing assay indicated accelerated wound closure upon GRP94 overexpression (Figures 3E and 3F). As anticipated, the Transwell assay revealed an increased number of HGC-27-GRP94 cells traversing the membrane, with or without matrigel (Figures 3G and 3H).

The YAP/TEAD1 axis promoted anoikis resistance, migration, and invasion of GC cells

Previous reports have highlighted the critical role of the Hippo-YAP pathway in cell adhesion.[21,22] Considering that the loss of cell adhesion between cells and between cells and the extracellular matrix can trigger anoikis, we focused on the Hippo/YAP pathway's involvement in this process, particularly its interaction with GRP94 in gastric cancer, which remains ambiguous and has recently garnered research attention. WB analysis revealed that shGRP94 cells exhibit increased phosphorylated YAP (pYAP) but decreased SP1 and TEAD1 compared to controls in

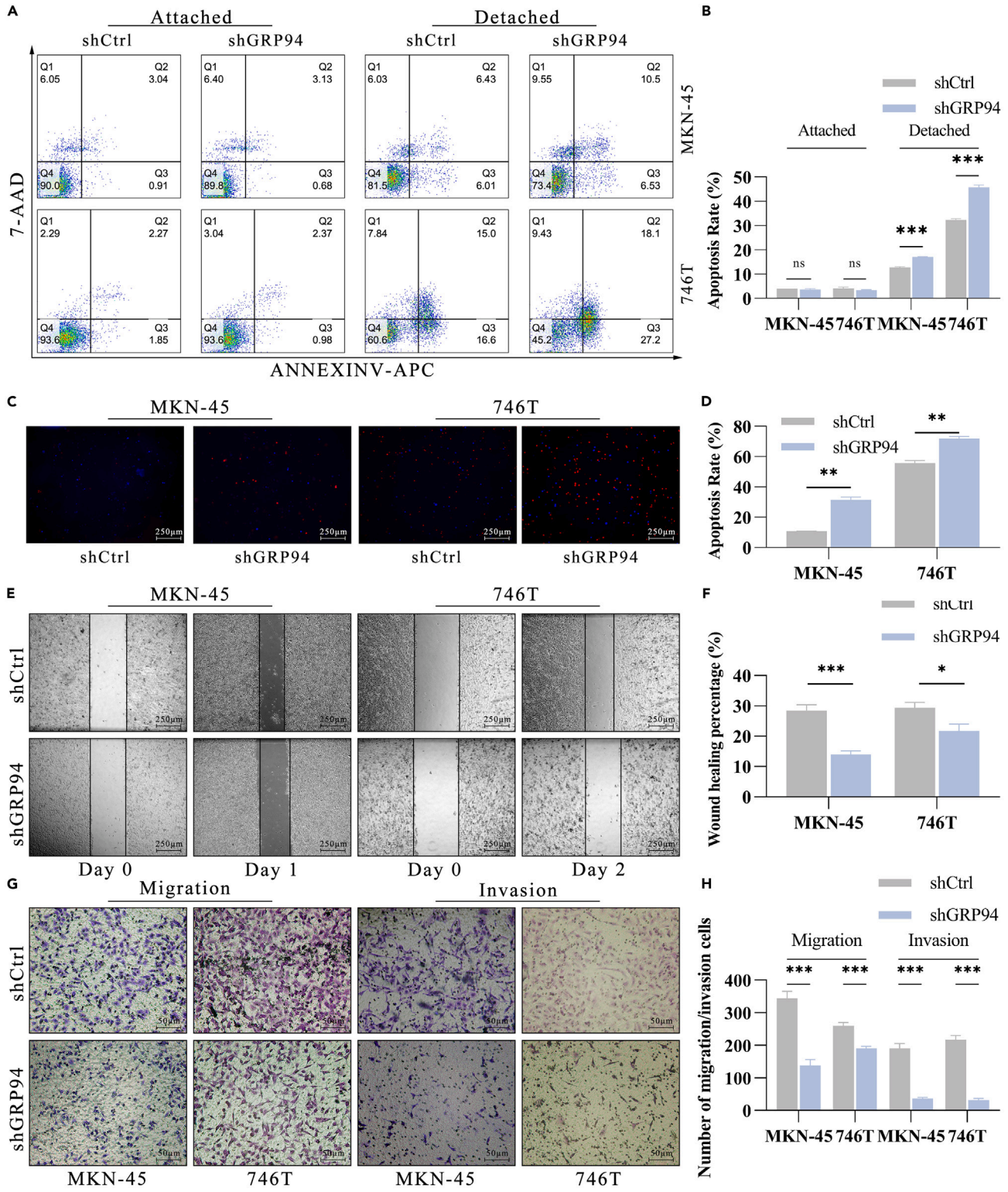

Figure 2. Knockdown of GRP94 suppressed anoikis resistance, migration, and invasion of GC cells in vitro

(A and B) GC cells underwent a culture in plates either precoated with poly-HEMA or without it for 48 h. Apoptosis rates in both attached and detached cells were assessed using flow cytometry, following staining with annexin V-APC/7-AAD. The experiment was repeated three times.

Figure 2. *Continued*

(C and D) Ethd-1/calcein blue AM staining was performed to assess the apoptosis rate of MKN-45 and 746T cells. The working concentrations of calcein blue AM and EthD-1 were 2 μM and 4 μM, respectively. Displayed images are at 20× magnification with a scale bar representing 250 μm.

(E and F) Wound closure was documented at 24 h (for MKN-45) or 48 h (for 746T). The black lines demarcate the wound boundaries. Displayed images are at 20× magnification with a scale bar representing 250 μm.

(G and H) Upon GRP94 knockdown, a decrease in the number of cells traversing the membrane was observed in both migration and invasion assays for MKN-45 and 746T cells. The images are magnified 100×, and the scale bar corresponds to 50 μm. (ns, $*p < 0.05$; $**p < 0.01$; $***p < 0.001$. Results are shown as mean ± SEM.).

MKN-45, 746T, and HGC-27 cells, while upregulated GRP94 resulted lower phosphorylated YAP (pYAP) but higher SP1 and TEAD1 levels (Figure 4A). Transcriptome sequencing revealed a significant downregulation of IL-6, targeting YAP/TEAD1 pathway[23,24] (Figure S2B). This was supported by Kyoto Encyclopedia of Genes and Genomes analysis and Gene Set Enrichment Analysis, showing an enrichment in cytokine-cytokine receptor interactions (Figures S2C and S2D), and corroborated by protein-protein interaction networks and ELISA, confirming GRP94's interaction with IL-6 (Figures S2E and S2F). GEPIA data indicates a moderate correlation between IL-6 and YAP/TEAD1 expression, which may partially explain the YAP/TEAD1 pathway suppression following GRP94 knockdown (Figure S2G). After knocking down IL-6 using siRNAs, the pYAP levels significantly increased, accompanied by the significant decrease in TEAD1 levels (Figures S2H and S2I). We employed verteporfin as an inhibitor and GA-017 as an activator of YAP. Verteporfin treatment increased phosphorylation of YAP at ser109, ser127, and ser397 sites, subsequently inhibiting TEAD1 expression, while GA017 inhibited YAP phosphorylation at ser109 and ser127 sites, enhancing TEAD1 expression (Figure 4B). Flow cytometry (FCM) and Ethd-1/calcein blue staining experiments revealed that reduced pYAP levels resulted in decreased anoikis, a trend that was reversed with increased pYAP levels (Figures 4C–4F). We also found that knocking down IL-6 (Figures S3A and S3B) or SP1 (Figures S3C–S3E) significantly increased the apoptosis rate of GC cells after suspended culture. Furthermore, verteporfin reduced, whereas GA-017 enhanced, the migration and invasion abilities of HGC-27-GRP94 and MKN-45-shGRP94 cells respectively, confirmed by wound healing (Figures 4G and 4H) and Transwell assays (Figures 4I and 4J).

GRP94 was observed to enhance the peritoneal metastasis of GC in xenograft mice models

Mice were injected intraperitoneally with either MKN-45-shGRP94 or MKN-45-shCtrl cells to evaluate the impact of GRP94 on GC metastasis. H&E staining is used to confirm the formation of tumors (Figure S3F). The shGRP94 group presented fewer metastatic nodules compared to the shCtrl group (Figures 5A and 5B). *In vivo* imaging system (IVIS) further revealed that the tumor burden in the shGRP94 group was less pronounced than in the shCtrl groups within the peritoneal region (Figures 5C and 5D). IHC staining demonstrated an elevated expression of E-cadherin and a reduced expression of N-cadherin in the shGRP94 group, confirming the inhibitory role of GRP94 knockdown on GC metastasis *in vivo* (Figure 5E).

DISCUSSION

GC is the fifth most commonly diagnosed cancer worldwide, with 768,793 recorded deaths in 2020.[25] A significant challenge in its clinical treatment is peritoneal metastasis. While GRP94 has been linked to metastatic GC, its molecular mechanism is not yet clearly understood. Our study delineates the relationship between GRP94 and the YAP/TEAD1 axis, which contributes to GC cells resistance to apoptosis, deepening our understanding of GRP94's role in metastatic GC (Figure 5F).

Elevated levels of GRP94 were observed in tumor tissues in comparison to adjacent normal tissues, correlating with poor progression. The process leading to peritoneal metastasis in GC is multifaceted. It is believed that GC cells, once detached from the primary tumor's extracellular matrix, resist apoptosis during metastasis and eventually colonize areas like the visceral peritoneum or omentum.[26] GRP94 plays a protective role in cells under stress and has been associated with poor outcomes in several cancer types.[27–29] However, its relationship with anoikis resistance in GC remained unexplored until now. Our findings indicated that while attached culture did not impact the apoptosis rate between shGRP94 and shCtrl groups, GRP94 knockdown weakened anoikis resistance, migration, and invasion abilities. This was further validated *in vivo* using a xenograft assay where GRP94 knockdown resulted in fewer abdominal metastases.

A significant aspect of our study was to identify the pathway through which GRP94 functions. Considering that integrins,[30,31] LRP6,[32] and GARP[33] are GRP94 clients, we attempted to explore whether integrins, LRP6-β-catenin, and GARP-TGF-β signaling are associated with GRP94 mediated resistance to anoikis and metastasis in GC cells. The results showed that knocking down GRP94 significantly reduced the protein levels of GARP, TGF-β1, and β-catenin in MKN-45 and 746T cells (Figure S4A).

Additionally, WB analysis also pointed to significant inhibition of YAP/TEAD1 pathway due to GRP94 knockdown, which has rarely been studied before. Although GRP94's primary function is aiding client proteins to achieve proper conformation,[34] our coIP failed to identify any direct interaction between GRP94 and YAP (Figure S4B), hinting at an indirect mechanism. Known YAP-TEAD inhibitor verteporfin has shown efficacy in reducing tumor metastasis and recurrence across various cancer types. For instance, verteporfin hindered tumor migration and invasion in preclinical GBM models,[35] while decreased YAP expression similarly suppressed metastasis in NSCLC cells.[36] Our results, using verteporfin and GA-017 (a YAP activator), were consistent with these findings. However, our study did not elucidate the specific mechanisms by which changes in the YAP pathway mediate resistance to anoikis. One possible explanation is the alteration of reactive oxygen species (ROS) levels. Previous studies have shown that ROS production significantly increases in breast epithelial cells after detachment from the extracellular matrix,[37] and excessive ROS is known to be associated with apoptosis. Recently, the relationship between ROS and the YAP pathway has gained attention. One study indicated that knocking down YAP in human aortic endothelial cells rescued the inhibition of ROS generation by CoQ10.[38] Conversely, another study demonstrated that chaetocin-induced ROS promoted glioma cell apoptosis by

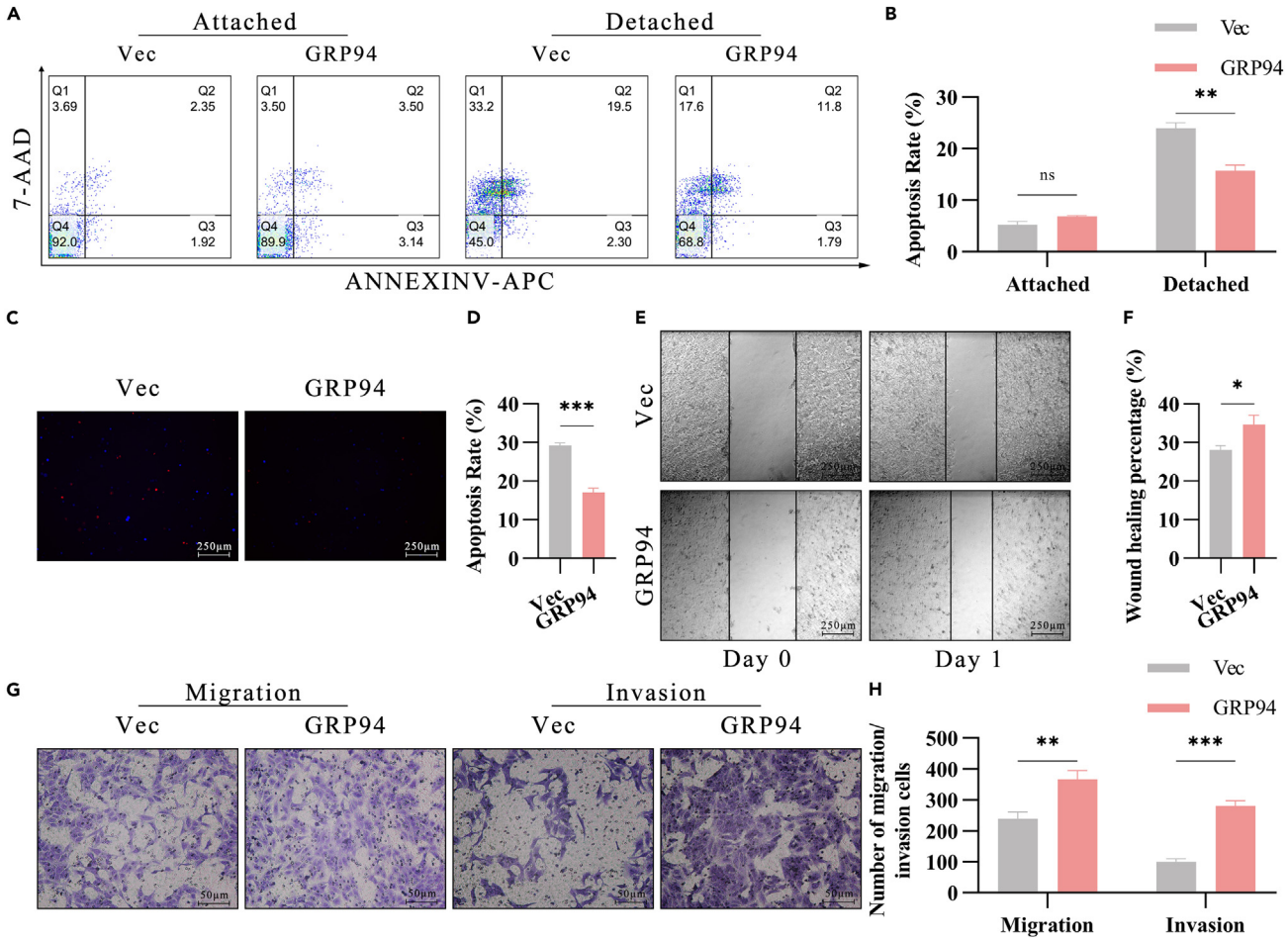

Figure 3. Overexpression of GRP94 enhanced anoikis resistance, migration and invasion in GC cells in vitro

(A and B) GC cells with elevated GRP94 levels were subjected to poly-HEMA treatment for 48 h. The apoptosis rate was determined using FCM. The experiment was repeated three times.

(C and D) Ethd-1/calcein blue AM staining was performed to assess the apoptosis rate of HGC-27 cells. The working concentrations of calcein blue AM and EthD-1 were 2 μM and 4 μM, respectively. Displayed images are at 20× magnification with a scale bar representing 250 μm.

(E and F) GRP94 overexpression improved the wound healing capabilities of HGC-27 cells, as visualized with a 20× magnification (scale bar: 250 μm).

(G and H) Transwell assays illustrated enhanced invasive and migratory aptitudes in HGC-27 cells due to GRP94 overexpression, visualized at 100× magnification (scale bar: 50 μm). (ns, *$p < 0.05$; **$p < 0.01$; ***$p < 0.001$. Results are shown as mean ± SEM.).

increasing YAP1 levels.[39] Given these conflicting perspectives, further investigation is necessary to explore the role of ROS in GRP94-mediated resistance to anoikis in gastric cancer cells through the YAP pathway.

In conclusion, our work unveiled the relationship between GRP94 and anoikis resistance in GC, shedding light on the underlying mechanisms of metastasis. The research breaks new ground by linking GRP94's function to the inhibition of the YAP/TEAD1 pathway, a novel finding in GC research, and opens new perspectives in understanding cancer progression and potential therapeutic approaches.

Limitations of the study

While a potential therapeutic target is identified, there are still gaps in our understanding. Notably, the cause behind the increase in YAP phosphorylation remains unexplored. Besides, future research should include more clinical samples of GC patients, especially those with peritoneal metastasis, for more comprehensive survival analysis, thereby enhancing our understanding of GC metastasis and potential therapeutic approaches.

STAR★METHODS

Detailed methods are provided in the online version of this paper and include the following:

- KEY RESOURCES TABLE

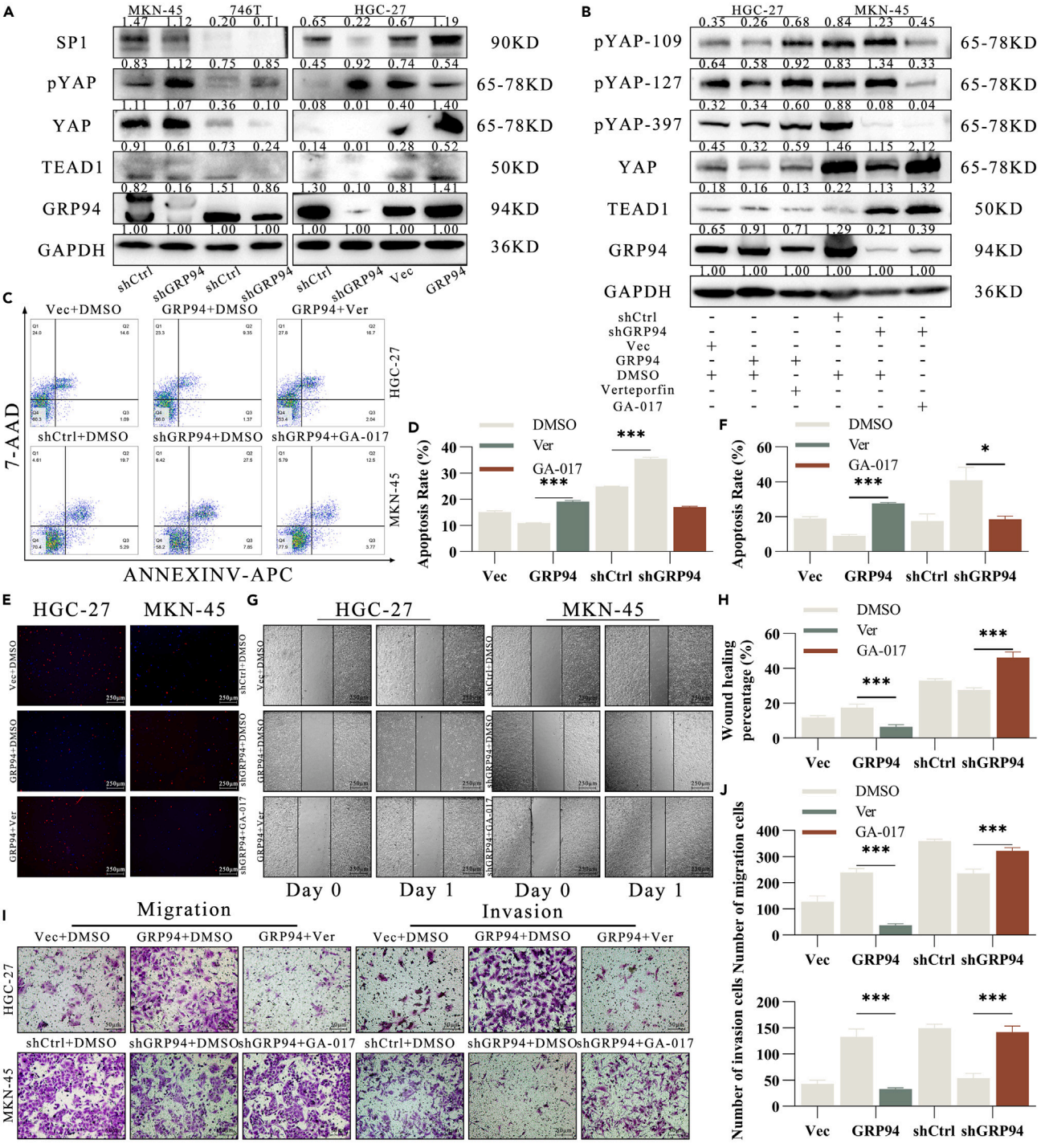

Figure 4. The YAP/TEAD1 axis promoted anoikis resistance, migration, and invasion of GC cells

(A) WB analysis revealed the inhibition of the YAP/TEAD1 pathway in MKN-45, 746T, and HGC-27 cells, as a consequence of GRP94 knockdown, while GRP94 overexpression activated the YAP/TEAD1 pathway in HGC-27 cells.

(B) Verteporfin increased YAP phosphorylation, reducing TEAD1 expression, while GA-017 had the opposite effect.

(C and D) Verteporfin (Ver) negated the anoikis resistance observed in HGC-27-GRP94 cells. Conversely, YAP activation increased the anoikis resistance in MKN-45-shGRP94 cells, as shown by FCM. The experiment was repeated three times.

Figure 4. *Continued*

(E and F) Ethd-1/calcein blue AM staining was performed to assess the apoptosis rate of HGC-27 and MKN-45 cells, with the application of verteporfin and GA-017. The working concentrations of calcein blue AM and EthD-1 were 2 μM and 4 μM, respectively. Displayed images are at 20× magnification with a scale bar representing 250 μm.

(G and H) A wound healing assay assessed the impact of YAP on GRP94 using verteporfin and GA-017. Scale bar: 250 μm at 20× magnification.

(I and J) Verteporfin mitigated the enhanced migration and invasion capacities of HGC-27 cells induced by GRP94. In contrast, GA-017 offset the migration and invasion inhibitions in MKN-45 cells caused by GRP94 downregulation. The scale bar, 50 μm, 100× magnification. (ns, $*p < 0.05$; $**p < 0.01$; $***p < 0.001$. Results are shown as mean ± SEM.).

- RESOURCE AVAILABILITY
  - Lead contact
  - Materials availability
  - Data and code availability
- EXPERIMENTAL MODEL AND STUDY PARTICIPANT DETAILS
  - Clinical patient samples
  - Animal tumor transplantation
- METHOD DETAILS
  - Cell line and culture
  - RNA isolation and quantitative real-time PCR
  - Protein extraction and western blotting
  - Virus transduction
  - RNA sequencing
  - Immunohistochemistry staining
  - Wound healing assay
  - Migration and invasion assays
  - Suspension culture of adherent cells
  - Flow cytometry analysis of apoptosis and anoikis
  - Ethd-1/Calcein Blue AM staining
  - Dual luciferase reporter assay
  - Chromatin immunoprecipitation assay
- QUANTIFICATION AND STATISTICAL ANALYSIS
  - Statistical analysis

SUPPLEMENTAL INFORMATION

Supplemental information can be found online at https://doi.org/10.1016/j.isci.2024.110638.

ACKNOWLEDGMENTS

We thank Guilherme Bauer Negrini and Vecteezy for their drawings. This work was supported by grants from the National Natural Science Foundation of China (grant no. 82173222 and 82072602), Science and Technology Commission of Shanghai Municipality (grant no. 20DZ2201900), and the Collaborative Innovation Center for Clinical and Translational Science by Chinese Ministry of Education & Shanghai (grant no. CCTS-2022202 and CCTS-202302). The funders had no role in study design, data collection and analysis, decision to publish, or preparation of the manuscript.

AUTHOR CONTRIBUTIONS

C.L. and Z.W. made contributions to the conception and design of the work. Q.S., Y.L., and Y.D. were executors of all the experiments. Data analysis was performed by R. Yang and R. Yan. Q.S. and Y.G. completed the original draft. C.L., Z.W., and Y.Y. completed the final revision. All authors read and approved the final manuscript.

DECLARATION OF INTERESTS

The authors declare no competing interests.

Received: December 21, 2023
Revised: May 30, 2024
Accepted: July 30, 2024
Published: August 7, 2024

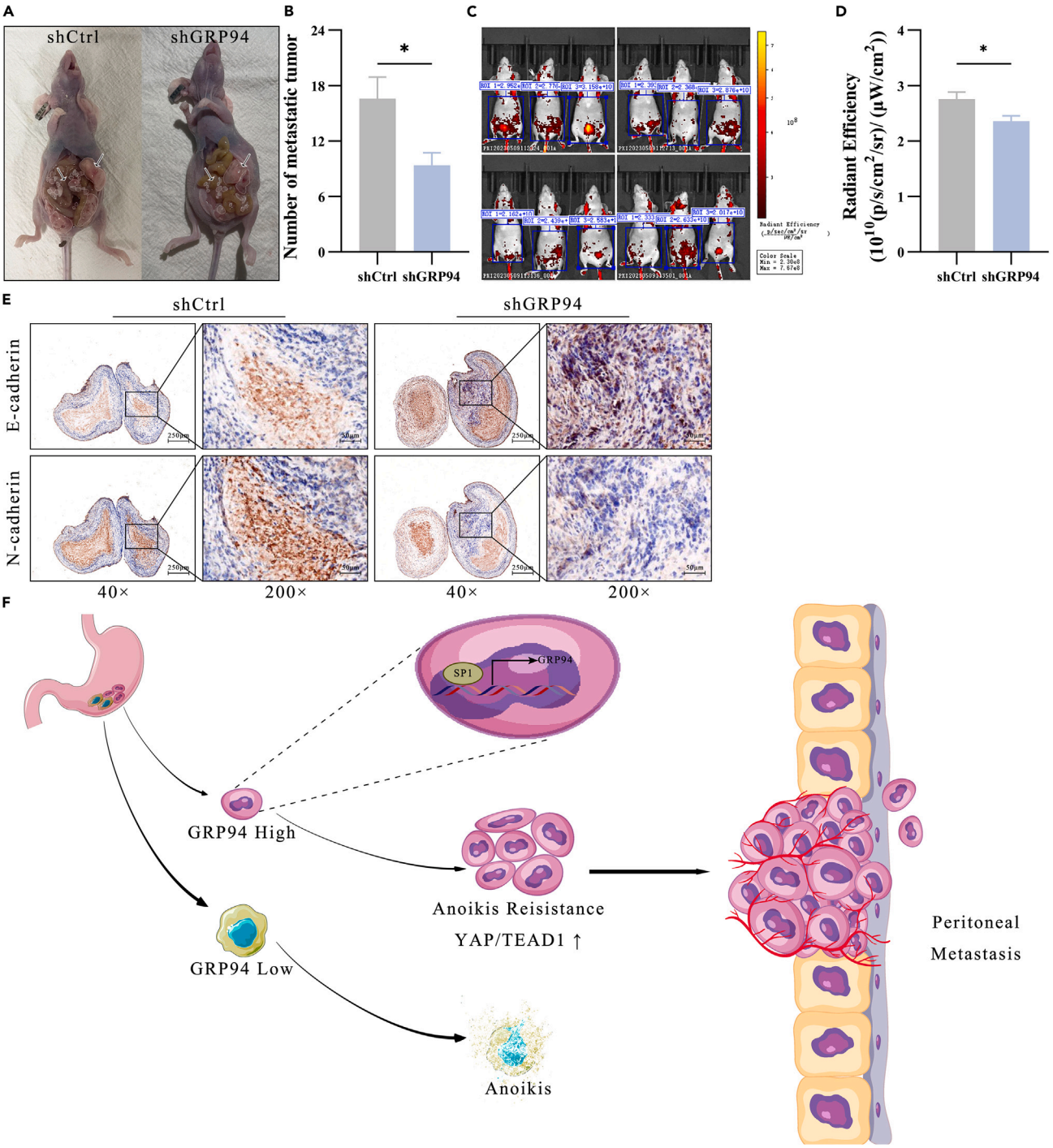

Figure 5. GRP94 was observed to enhance the peritoneal metastasis of GC in xenograft mice models

(A and B) GFP-labeled MKN-45-shCtrl and MKN-45-shGRP94 cells were intraperitoneally injected into two groups of six nude mice each. The subsequent count revealed the number of metastatic tumors (white arrows and lines).

(C and D) Using IVIS, total radiant efficiency was determined, with regions of interest highlighted by blue boxes in the image.

(E) Upon sacrificing the mice, potential tumor nodules were harvested from them and analyzed for E-cadherin and N-cadherin expression using IHC.

(F) A schematic illustrates the proposed mechanism through which GRP94 promotes GC progression. (ns, $*p < 0.05$; $**p < 0.01$; $***p < 0.001$. Results are shown as mean ± SEM).

REFERENCES

1. Van Cutsem, E., Sagaert, X., Topal, B., Haustermans, K., and Prenen, H. (2016). Gastric cancer. Lancet *388*, 2654–2664. https://doi.org/10.1016/S0140-6736(16)30354-3.
2. Chen, W., Zheng, R., Zeng, H., Zhang, S., and He, J. (2015). Annual report on status of cancer in China, 2011. Chin. J. Cancer Res. *27*, 2–12. https://doi.org/10.3978/j.issn.1000-9604.2015.01.06.
3. Siegel, R.L., Miller, K.D., and Jemal, A. (2019). Cancer statistics, 2019. CA. Cancer J. Clin. *69*, 7–34. https://doi.org/10.3322/caac.21551.
4. Cao, Z., Livas, T., and Kyprianou, N. (2016). Anoikis and EMT: Lethal "Liaisons" during Cancer Progression. Crit. Rev. Oncog. *21*, 155–168. https://doi.org/10.1615/CritRevOncog.2016016955.
5. Wang, Y., Chen, H., Liu, W., Yan, H., Zhang, Y., Cheung, A.H.K., Zhang, J., Chen, B., Liang, L., Zhou, Z., et al. (2022). MCM6 is a critical transcriptional target of YAP to promote gastric tumorigenesis and serves as a therapeutic target. Theranostics *12*, 6509–6526. https://doi.org/10.7150/thno.75431.
6. Liu, Z., Li, J., Ding, Y., Ma, M., Chen, J., Lei, W., Li, L., Yao, Y., Yu, X., Zhong, M., et al. (2022). USP49 mediates tumor progression and poor prognosis through a YAP1-dependent feedback loop in gastric cancer. Oncogene *41*, 2555–2570. https://doi.org/10.1038/s41388-022-02267-0.
7. Yue, T., Tian, A., and Jiang, J. (2012). The Cell Adhesion Molecule Echinoid Functions as a Tumor Suppressor and Upstream Regulator of the Hippo Signaling Pathway. Dev. Cell *22*, 255–267. https://doi.org/10.1016/j.devcel.2011.12.011.
8. Ohta, Y., Fujii, M., Takahashi, S., Takano, A., Nanki, K., Matano, M., Hanyu, H., Saito, M., Shimokawa, M., Nishikori, S., et al. (2022). Cell-matrix interface regulates dormancy in human colon cancer stem cells. Nature *608*, 784–794. https://doi.org/10.1038/s41586-022-05043-y.
9. Yu, S.-J., Hu, J.-Y., Kuang, X.-Y., Luo, J.-M., Hou, Y.-F., Di, G.-H., Wu, J., Shen, Z.-Z., Song, H.-Y., and Shao, Z.-M. (2013). MicroRNA-200a Promotes Anoikis Resistance and Metastasis by Targeting YAP1 in Human Breast Cancer. Clin. Cancer Res. *19*, 1389–1399. https://doi.org/10.1158/1078-0432.CCR-12-1959.
10. Haemmerle, M., Taylor, M.L., Gutschner, T., Pradeep, S., Cho, M.S., Sheng, J., Lyons, Y.M., Nagaraja, A.S., Dood, R.L., Wen, Y., et al. (2017). Platelets reduce anoikis and promote metastasis by activating YAP1 signaling. Nat. Commun. *8*, 310. https://doi.org/10.1038/s41467-017-00411-z.
11. Pugh, K.W., Alnaed, M., Brackett, C.M., and Blagg, B.S.J. (2022). The biology and inhibition of glucose-regulated protein 94/gp96. Med. Res. Rev. *42*, 2007–2024. https://doi.org/10.1002/med.21915.
12. Lee, A.S. (2014). Glucose-regulated proteins in cancer: molecular mechanisms and therapeutic potential. Nat. Rev. Cancer *14*, 263–276. https://doi.org/10.1038/nrc3701.
13. Howard, E.W., Leung, S.C.L., Yuen, H.F., Chua, C.W., Lee, D.T., Chan, K.W., Wang, X., and Wong, Y.C. (2008). Decreased adhesiveness, resistance to anoikis and suppression of GRP94 are integral to the survival of circulating tumor cells in prostate cancer. Clin. Exp. Metastasis *25*, 497–508. https://doi.org/10.1007/s10585-008-9157-3.
14. Li, C., Tang, Z., Zhang, W., Ye, Z., and Liu, F. (2021). GEPIA2021: integrating multiple deconvolution-based analysis into GEPIA. Nucleic Acids Res. *49*, W242–W246. https://doi.org/10.1093/nar/gkab418.
15. Woo, S.M., Seo, S.U., Min, K.-J., and Kwon, T.K. (2022). Melatonin induces apoptotic cell death through Bim stabilization by Sp1-mediated OTUD1 upregulation. J. Pineal Res. *72*, e12781. https://doi.org/10.1111/jpi.12781.
16. Yang, W.-B., Hsu, C.-C., Hsu, T.-I., Liou, J.-P., Chang, K.-Y., Chen, P.-Y., Liu, J.-J., Yang, S.-T., Wang, J.-Y., Yeh, S.-H., et al. (2020). Increased activation of HDAC1/2/6 and Sp1 underlies therapeutic resistance and tumor growth in glioblastoma. Neuro Oncol. *22*, 1439–1451. https://doi.org/10.1093/neuonc/noaa103.
17. Wang, P., Song, Y., Li, H., Zhuang, J., Shen, X., Yang, W., Mi, R., Lu, Y., Yang, B., Ma, M., and Shen, H. (2023). SIRPA enhances osteosarcoma metastasis by stabilizing SP1 and promoting SLC7A3-mediated arginine uptake. Cancer Lett. *576*, 216412. https://doi.org/10.1016/j.canlet.2023.216412.
18. Zhang, X., Li, F., Zhou, Y., Mao, F., Lin, Y., Shen, S., Li, Y., Zhang, S., and Sun, Q. (2021). Long noncoding RNA AFAP1-AS1 promotes tumor progression and invasion by regulating the miR-2110/Sp1 axis in triple-negative breast cancer. Cell Death Dis. *12*, 627. https://doi.org/10.1038/s41419-021-03917-z.
19. Kim, Y.-N., Koo, K.H., Sung, J.Y., Yun, U.-J., and Kim, H. (2012). Anoikis resistance: an essential prerequisite for tumor metastasis. Int. J. Cell Biol. *2012*, 306879. https://doi.org/10.1155/2012/306879.
20. Bhat, A.A., Yousuf, P., Wani, N.A., Rizwan, A., Chauhan, S.S., Siddiqi, M.A., Bedognetti, D., El-Rifai, W., Frenneaux, M.P., Batra, S.K., et al. (2021). Tumor microenvironment: an evil nexus promoting aggressive head and neck squamous cell carcinoma and avenue for targeted therapy. Signal Transduct. Tar. *6*, 12. https://doi.org/10.1038/s41392-020-00419-w.
21. Fard, D., Testa, E., Panzeri, V., Rizzolio, S., Bianchetti, G., Napolitano, V., Masciarelli, S., Fazi, F., Maulucci, G., Scicchitano, B.M., et al. (2023). SEMA6C: a novel adhesion-independent FAK and YAP activator, required for cancer cell viability and growth. Cell. Mol. Life Sci. *80*, 111. https://doi.org/10.1007/s00018-023-04756-1.
22. Rogg, M., Maier, J.I., Helmstädter, M., Sammarco, A., Kliewe, F., Kretz, O., Weißer, L., Van Wymersch, C., Findeisen, K., Koessinger, A.L., et al. (2023). A YAP/TAZ-ARHGAP29-RhoA Signaling Axis Regulates Podocyte Protrusions and Integrin Adhesions. Cells *12*, 1795. https://doi.org/10.3390/cells12131795.
23. Azar, W.J., Christie, E.L., Mitchell, C., Liu, D.S., Au-Yeung, G., and Bowtell, D.D.L. (2020). Noncanonical IL6 Signaling-Mediated Activation of YAP Regulates Cell Migration and Invasion in Ovarian Clear Cell Cancer. Cancer Res. *80*, 4960–4971. https://doi.org/10.1158/0008-5472.CAN-19-3044.
24. Symons, R.A., Colella, F., Collins, F.L., Rafipay, A.J., Kania, K., McClure, J.J., White, N., Cunningham, I., Ashraf, S., Hay, E., et al. (2022). Targeting the IL-6-Yap-Snail signalling axis in synovial fibroblasts ameliorates inflammatory arthritis. Ann. Rheum. Dis. *81*, 214–224. https://doi.org/10.1136/annrheumdis-2021-220875.
25. Sung, H., Ferlay, J., Siegel, R.L., Laversanne, M., Soerjomataram, I., Jemal, A., and Bray, F. (2021). Global Cancer Statistics 2020: GLOBOCAN Estimates of Incidence and Mortality Worldwide for 36 Cancers in 185 Countries. CA. Cancer J. Clin. *71*, 209–249. https://doi.org/10.3322/caac.21660.
26. Wang, Z., Chen, J.-Q., Liu, J.-L., and Tian, L. (2019). Issues on peritoneal metastasis of gastric cancer: an update. World J. Surg. Oncol. *17*, 215. https://doi.org/10.1186/s12957-019-1761-y.
27. Hao, M., Guo, Y., Zhang, Z., Zhou, H., Gu, Q., and Xu, J. (2022). 6-acrylic phenethyl ester-2-pyranone derivative induces apoptosis and G2/M arrest by targeting GRP94 in colorectal cancer. Bioorg. Chem. *123*, 105802. https://doi.org/10.1016/j.bioorg.2022.105802.
28. Kim, S.-H., Ji, J.H., Park, K.T., Lee, J.H., Kang, K.W., Park, J.H., Hwang, S.W., Lee, E.H., Cho, Y.J., Jeong, Y.Y., et al. (2015). High-level expression of Hsp90β is associated with poor survival in resectable non-small-cell lung cancer patients. Histopathology *67*, 509–519. https://doi.org/10.1111/his.12675.
29. Zhang, B., Ayuda-Durán, P., Piechaczyk, L., Fløisand, Y., Safont, M.M., Karlsen, I.T., Fandalyuk, Z., Tadele, D., van Mierlo, P., Rowe, A.D., et al. (2019). GRP94 rewires and buffers the FLT3-ITD signaling network and promotes survival of acute myeloid leukemic stem cells. Haematologica *104*, e229. https://doi.org/10.3324/haematol.2019.220533.
30. Ghosh, S., Shinogle, H.E., Galeva, N.A., Dobrowsky, R.T., and Blagg, B.S.J. (2016). Endoplasmic Reticulum-resident Heat Shock Protein 90 (HSP90) Isoform Glucose-regulated Protein 94 (GRP94) Regulates Cell Polarity and Cancer Cell Migration by Affecting Intracellular Transport. J. Biol. Chem. *291*, 8309–8323. https://doi.org/10.1074/jbc.M115.688374.
31. Staron, M., Yang, Y., Liu, B., Li, J., Shen, Y., Zúñiga-Pflücker, J.C., Aguila, H.L., Goldschneider, I., and Li, Z. (2010). gp96, an endoplasmic reticulum master chaperone for integrins and Toll-like receptors, selectively regulates early T and B lymphopoiesis. Blood *115*, 2380–2390. https://doi.org/10.1182/blood-2009-07-233031.
32. Liu, B., Staron, M., Hong, F., Wu, B.X., Sun, S., Morales, C., Crosson, C.E., Tomlinson, S., Kim, I., Wu, D., and Li, Z. (2013). Essential roles of grp94 in gut homeostasis via chaperoning canonical Wnt pathway. Proc. Natl. Acad. Sci. USA *110*, 6877–6882. https://doi.org/10.1073/pnas.1302933110.
33. Zhang, Y., Wu, B.X., Metelli, A., Thaxton, J.E., Hong, F., Rachidi, S., Ansa-Addo, E., Sun, S., Vasu, C., Yang, Y., et al. (2015). GP96 is a GARP chaperone and controls regulatory T cell functions. J. Clin. Invest. *125*, 859–869. https://doi.org/10.1172/JCI79014.
34. Kotler, J.L.M., and Street, T.O. (2023). Mechanisms of Protein Quality Control in the Endoplasmic Reticulum by a Coordinated Hsp40-Hsp70-Hsp90 System. Annu. Rev. Biophys. *52*, 509–524. https://doi.org/10.1146/annurev-biophys-111622-091309.
35. Barrette, A.M., Ronk, H., Joshi, T., Mussa, Z., Mehrotra, M., Bouras, A., Nudelman, G., Jesu Raj, J.G., Bozec, D., Lam, W., et al. (2022). Anti-invasive efficacy and survival benefit of the YAP-TEAD inhibitor verteporfin in preclinical glioblastoma models. Neuro

Oncol. *24*, 694–707. https://doi.org/10.1093/neuonc/noab244.

36. Takeda, T., Tsubaki, M., Genno, S., Matsuda, T., Yamamoto, Y., Kimura, A., Shimizu, N., and Nishida, S. (2022). Inhibition of yes-associated protein suppresses migration, invasion, and metastasis in non-small cell lung cancer in vitro and in vivo. Clin. Exp. Med. *22*, 221–228. https://doi.org/10.1007/s10238-021-00738-4.

37. Kamarajugadda, S., Cai, Q., Chen, H., Nayak, S., Zhu, J., He, M., Jin, Y., Zhang, Y., Ai, L., Martin, S.S., et al. (2013). Manganese superoxide dismutase promotes anoikis resistance and tumor metastasis. Cell Death Dis. *4*, e504. https://doi.org/10.1038/cddis.2013.20.

38. Xie, T., Wang, C., Jin, Y., Meng, Q., Liu, Q., Wu, J., and Sun, H. (2020). CoenzymeQ10-Induced Activation of AMPK-YAP-OPA1 Pathway Alleviates Atherosclerosis by Improving Mitochondrial Function, Inhibiting Oxidative Stress and Promoting Energy Metabolism. Front. Pharmacol. *11*, 1034. https://doi.org/10.3389/fphar.2020.01034.

39. Dixit, D., Ghildiyal, R., Anto, N.P., and Sen, E. (2014). Chaetocin-induced ROS-mediated apoptosis involves ATM-YAP1 axis and JNK-dependent inhibition of glucose metabolism. Cell Death Dis. *5*, e1212. https://doi.org/10.1038/cddis.2014.179.

40. Wang, Z., Ma, X., Cai, Q., Wang, X., Yu, B., Cai, Q., liu, B., Zhu, Z., and Li, C. (2014). MiR-199a-3p promotes gastric cancer progression by targeting ZHX1. FEBS Lett. *588*, 4504–4512. https://doi.org/10.1016/j.febslet.2014.09.047.

41. Pan, T., Yu, Z., Jin, Z., Wu, X., Wu, A., Hou, J., Chang, X., Fan, Z., Li, J., Yu, B., et al. (2021). Tumor suppressor lnc-CTSLP4 inhibits EMT and metastasis of gastric cancer by attenuating HNRNPAB-dependent Snail transcription. Mol. Ther. Nucleic Acids *23*, 1288–1303. https://doi.org/10.1016/j.omtn.2021.02.003.

42. Wang, Z.Q., Cai, Q., Hu, L., He, C.Y., Li, J.F., Quan, Z.W., Liu, B.Y., Li, C., and Zhu, Z.G. (2017). Long noncoding RNA UCA1 induced by SP1 promotes cell proliferation via recruiting EZH2 and activating AKT pathway in gastric cancer. Cell Death Dis. *8*, e2839. https://doi.org/10.1038/cddis.2017.143.

STAR★METHODS

KEY RESOURCES TABLE

REAGENT or RESOURCE	SOURCE	IDENTIFIER
Antibodies		
anti-GRP94	Abcam	Cat#Ab238126; RRID: AB_3271551
anti-YAP	CST	Cat#14074; RRID: AB_2650491
anti-YAP-109	CST	Cat#53749; RRID: AB_2799445
anti-YAP-127	CST	Cat#13008; RRID: AB_2650553
anti-YAP-397	CST	Cat#13619; RRID: AB_2650554
anti-SP1	ABclonal	Cat#A19649; RRID: AB_2862714
anti-TEAD1	ABclonal	Cat#A5218; RRID: AB_2863490
anti-ITGB3	ABclonal	Cat#A19073; RRID: AB_2862565
anti- ITGB4	ABclonal	Cat#A4596; RRID: AB_2863306
anti-GARP	Proteintech	Cat#26021-1-AP; RRID: AB_2880339
anti-TGF-β1	ABclonal	Cat#A25313; RRID: AB_3271553
anti-LRP6	ABclonal	Cat#A22661; RRID: AB_3271554
anti-β-Catenin	ABclonal	Cat#A19657; RRID: AB_2862719
anti-GAPDH	Proteintech	Cat#HRP-60004; RRID: AB_2737588
Biological samples		
Human stomach samples	Ruijin Hospital, Shanghai Jiao Tong University School of medicine	N/A
Chemicals, peptides, and recombinant proteins		
RIPA lysis buffer	Invitrogen	Cat#89900
Protease Inhibitor Cocktail	MCE	Cat#HY-K0010
Phosphatase Inhibitor Cocktails I	MCE	Cat#HY-K0021
Phosphatase Inhibitor Cocktails II	MCE	Cat#HY-K0022
Phosphatase Inhibitor Cocktails III	MCE	Cat#HY-K0023
super sensitive ECL luminescence reagent	Meilunbio	Cat#MA0186
puromycin	Yeasen Biotechnology	Cat#60209ES10
matrigel	Corning	Cat#354234
Annexin V-APC	BD Biosciences	Cat#550474
7-AAD	BD Biosciences	Cat#559925
Calcein Blue AM	Abcam	Cat#Ab275490
EthD-1	Abbkine	Cat#BMD0060
Critical commercial assays		
RNA-Quick Purification Kit	ES Science	Cat#RN001
HiScript III RT SuperMix	Vazyme	Cat #R333
ChamQ Universal SYBR qPCR Master Mix	Vazyme	Cat #Q711
Deposited data		
RNA sequencing data for GRP94 knockdown	GEO Database	GEO: GSE267811
Experimental models: Cell lines		
MKN-45	Dr. Yu Beiqin, Shanghai Jiao Tong University School of Medicine	N/A
746T	Procell	Cat #CL-0115

(*Continued on next page*)

Continued

REAGENT or RESOURCE	SOURCE	IDENTIFIER
MGC-803	Shanghai Key Laboratory of Gastric Neoplasms, Ruijin Hospital	N/A
HGC-27	Dr. Su Liping, Shanghai Jiao Tong University School of Medicine	N/A
NCI-N87	Shanghai Key Laboratory of Gastric Neoplasms, Ruijin Hospital	N/A
GES-1	Shanghai Key Laboratory of Gastric Neoplasms, Ruijin Hospital	N/A
Experimental models: Organisms/strains		
BALB/c-nude mice	Cyagen Biosciences	Cat #C001217
Oligonucleotides		
Primer: GRP94 F: TATTCATCACAGACGACTTC	This paper	N/A
Primer: GRP94 R: GCTTCTTCCTAATCACCTTA	This paper	N/A
Primer: GAPDH F: GTCTCCTCTGACTTCAACAGCG	This paper	N/A
Primer: GAPDH R: ACCACCCTGTTGCTGTAGCCAA	This paper	N/A
Primer for ChIP: GRP94 F: CACGAATGGCTAGGATCCCC	This paper	N/A
Primer for ChIP: GRP94 R: TAGTCCATGACGCAAGCGAG	This paper	N/A
Software and algorithms		
ImageJ	ImageJ	RRID: SCR_003070
Image Pro Plus	Media Cybernetics	RRID:SCR_007369
FlowJo	BD Biosciences	RRID:SCR_008520
Graphpad Prism	GraphPad Software	RRID:SCR_002798

RESOURCE AVAILABILITY

Lead contact

Further information and requests for resources and reagents should be directed to and will be fulfilled by the lead contact, Chen Li (leedoctor@sina.com).

Materials availability

This study did not generate new unique reagents.

Data and code availability

- RNA sequencing data have been deposited at GEO and are publicly available as of the date of publication. Accession numbers are listed in the key resources table.
- This paper does not report original code.
- Any additional information required to reanalyze the data reported in this paper is available from the lead contact upon request.

EXPERIMENTAL MODEL AND STUDY PARTICIPANT DETAILS

Clinical patient samples

Forty pairs of GC tissues and adjacent non-tumor tissues were procured from Ruijin Hospital, Shanghai Jiao Tong University School of medicine. All participants identified racially as Asian and ethnically as Han Chinese, which is the predominant ethnic group in China. All samples came from patients who hadn't undergone therapy. Informed consent was obtained prior to sample collection. This experiment was

approved by the Ethics Committee of Shanghai Jiaotong University, School of Medicine Affiliated Ruijin Hospital. Subsequently, samples were fixed with 4% Paraformaldehyde in preparation for IHC staining.

Animal tumor transplantation

6-week-old female BALB/c-nude mice were sourced from Cyagen Biosciences (Taicang, China) and housed accordingly. Cell lines MKN-45-shGRP94-Ctrl and MKN-45-shGRP94 were prepared using trypsin and then resuspended in PBS. These cells were subsequently introduced into the mice's abdominal cavity (5×10^6 cells/150 μL/mouse). Tumor development and metastasis were monitored utilizing optical *in vivo* imaging (PerkinElmer IVIS Lumina Series III, Waltham, MA, USA). At the culmination of 40 days, all mice were humanely euthanized, documented, and peritoneal metastasis nodules were counted. Our experiments were sanctioned by the Institutional Laboratory Animal Ethics Committee (TACU23-FY019).

METHOD DETAILS

Cell line and culture

GC cell lines MKN-45, 746T, MGC-803, HGC-27, NCI-N87, and GES-1 were consistently maintained in our laboratory. Cells were cultured in Dulbecco's Modified Eagle Medium (containing Ala-Gln) supplemented with 10% FBS (Gibco, Carlsbad, CA, USA), 1% Penicillin/Streptomycin (Meilunbio, Dalian, Liaoning, China), and kept at 37°C in an incubator with a 5% CO2 atmosphere.

RNA isolation and quantitative real-time PCR

Total RNA was extracted using the RNA-Quick Purification Kit (ES Science, Shanghai, China), followed by reverse transcription into cDNA using the HiScript III RT SuperMix (Vazyme, Nanjing, Jiangsu, China). Quantitative real-time PCR (real-time qPCR) was then carried out using the ChamQ Universal SYBR qPCR Master Mix (Vazyme, Nanjing, Jiangsu, China), adhering to the provided protocol. The primer sequences for real-time qPCR included: GRP94-Forward (TATTCATCACAGACGACTTC), GRP94-Reverse (GCTTCTTCCTAATCACCTTA), GAPDH-Forward (GTCTCCTCTGACTTCAACAGCG), and GAPDH -Reverse (ACCACCCTGTTGCTGTAGCCAA). Relative expression of RNA normalized to GAPDH was calculated using $2^{-(\Delta\Delta Ct)}$ method.

Protein extraction and western blotting

Cells underwent lysis using the RIPA lysis buffer (Invitrogen, Carlsbad, CA, USA) combined with Protease Inhibitor Cocktail and Phosphatase Inhibitor Cocktails I, II, and III (all from MCE, Shanghai, China). The protein concentration in the lysates was determined through the BCA method. Western blotting (WB) procedures were executed based on our laboratory's established protocols.[40] Specific antibodies were employed for antigen detection, including anti-GRP94 (Abcam, Cat#Ab238126), anti-YAP (CST, Cat#14074), anti-YAP-109 (CST, Cat#53749), anti-YAP-127 (CST, Cat#13008), anti-YAP-397 (CST, Cat#13619), anti-SP1 (ABclonal, Cat#A19649), anti-TEAD1 (ABclonal, Cat#A5218), anti-ITGB3 (ABclonal, Cat#A19073), anti- ITGB4 (ABclonal, Cat#A4596), anti-GARP (Proteintech, Cat#26021-1-AP), anti-TGF-β1 (ABclonal, Cat#A25313), anti-LRP6 (ABclonal, Cat#A22661), anti-β-Catenin (ABclonal, Cat#A19657), anti-GAPDH (Proteintech, Cat#HRP-60004). Visualization of the reaction was achieved using a Tacon imaging system, complemented by the super sensitive ECL luminescence reagent (Meilunbio, Dalian, Liaoning, China). Densitometric analysis for blots was performed by ImageJ software.

Virus transduction

For virus transduction, cells underwent transfection using lentivirus and polybrene. Following this, they were screened with 5 μg/mL puromycin (Yeasen Biotechnology, Shanghai, China) as per the manufacturer's guidelines to establish stable cell lines. A week post-transfection, *GRP94* expression was validated using real-time qPCR and WB in preparation for subsequent experiments.

RNA sequencing

Total RNA was extracted from samples using TRIzol (Invitrogen, Carlsbad, CA, USA) according to the manufacturer's instructions. Sequencing was conducted on an Illumina Novaseq 6000 platform. Differential expression analysis of genes was performed with DESeq2, setting a threshold of Q value <0.05 and a fold change >2 or <0.5 for significant differential expression. For pathway analysis, differentially expressed genes (DEGs) were analyzed for KEGG pathway enrichment using R (version 4.2.2), and Gene Set Enrichment Analysis (GSEA) was carried out using GSEA software.

Immunohistochemistry staining

Immunohistochemistry (IHC) staining was conducted on paraffin sections which were deparaffinized in xylene and rehydrated in a graded ethanol series. Antigen retrieval was performed using citrate buffer (pH 6.0) and microwave heating. Sections were blocked with 3% BSA and incubated with primary antibody overnight at 4°C, followed by an HRP-conjugated secondary antibody. DAB was used for color development, and nuclei were counterstained with hematoxylin.[41] GRP94 protein levels were deduced by averaging the density (Integrated optical density (IOD)/Area) using Image Pro Plus software. Samples with high expression were categorized as tumor tissues showcasing higher GRP94 protein concentrations than what is considered normal.

Wound healing assay

Cells from MKN-45-shGRP94, 746T-shGRP94, and HGC-27-GRP94, as well as their respective negative control cell lines, were prepared in single cell suspensions and placed in 6-well plates. Wounds were introduced using 20 μL pipette tips, with photographs taken at intervals: 0, 1, and 2 days. Each experiment was conducted thrice.

Migration and invasion assays

For the migration assay, 700 μL of DMEM infused with 10% FBS was added to the lower chamber (Corning, Cat#3422, New York, NY, USA). Between 6 and 20×10^5 cells from the aforementioned cell lines, resuspended in 300 μL of serum-free DMEM, were added to the upper chamber. The setup was left for incubation between 24 and 72 h.

Regarding the invasion assay, the same volume of DMEM was added to the lower chamber. Cells, prepared similarly, were added to the upper chamber, which was pre-treated with 50 μL of matrigel (Corning, Cat#354234, New York, NY, USA). The subsequent incubation period also spanned 24–72 h.

Post-incubation, cells were treated with methanol for 30 min, stained using 0.1% crystal violet, and examined under 100× magnification. Quantification of the cells was achieved via ImageJ software.

Suspension culture of adherent cells

10 mg/mL poly-HEMA ethanol solution was evenly spread in a sterilized 6-well plate, using 400 μL per well. This action was repeated once the ethanol evaporated. Post three PBS washes, GC cells, treated with trypsin to create a single cell suspension, were transferred to the poly-HEMA coated plate. Their suspension culture was subsequently observed.

Flow cytometry analysis of apoptosis and anoikis

GC cells, post a 48-h suspension culture, were prepared for flow cytometry (FCM) analysis. Staining was done using Annexin V-APC (BD Biosciences, Cat#550474, NJ, USA) and 7-AAD (BD Biosciences, Cat#559925, NJ, USA). And a following analysis was conducted with the flow cytometer (BD Biosciences, NJ, USA). We calculated the apoptosis rate by summing the results from the Q2 and Q3 quadrants.

Ethd-1/Calcein Blue AM staining

Suspended GC cells were collected and centrifuged, and washed 3 times with PBS. Then, the cells were resuspended with a working concentration of 2 μM of Calcein Blue AM (Abcam, Cat#Ab275490) and 4 μM of EthD-1 (Abbkine, Cat#BMD0060) solution, and the cell density was adjusted to 5 × 10^6/mL. After incubating in the dark for 20 min at room temperature, the cells were washed 3 times with PBS again, and then observed and photographed using a fluorescence microscope.

Dual luciferase reporter assay

The human wild type and mutant GRP94 promoter regions (103928410–103930459) were integrated into the pGL3-basic vector, with pcDNA3.1-SP1 procured from Genomeditech (Shanghai, China). To explore the interplay between SP1 and GRP94, HGC-27 cells were seeded in 24-well plates. These cells were then co-transfected with either wild-type or mutant GRP94 promoter luciferase reporter plasmids, pRL-TK vector, and either pcDNA3.1- SP1 or pcDNA3.1.

Chromatin immunoprecipitation assay

Chromatin immunoprecipitation (ChIP) assays were conducted by lysing cells in 1 mL of ChIP Lysis Buffer, followed by sonication to shear DNA (30 s on, 30 s off, 99% power, total 30 min). The lysates were centrifuged at 12,000 rpm for 10 min at 4°C to collect the supernatant. For immunoprecipitation, 50 μL of supernatant was saved as input control and 450 μL was incubated with TEAD1 or Rabbit IgG antibodies at 4°C overnight. The antibody-bound complexes were captured with Protein G magnetic beads, washed, and the DNA was eluted and purified.[42] The primer sequences for the following real-time qPCR included: GRP94-Forward (CACGAATGGCTAGGATCCCC), GRP94-Reverse (TAGTCCATGACGCAAGCGAG).

QUANTIFICATION AND STATISTICAL ANALYSIS

Statistical analysis

Statistical evaluations were performed using the two-tailed Student's t test through GraphPad Prism 8 (GraphPad Software, LaJolla, CA, USA). A significance level of 0.05 was predetermined. Asterisks in results represent levels of statistical significance (*$p < 0.05$, **$p < 0.01$, ***$p < 0.001$).